J MATER SCI **41** (2006) 2729–2737

The impact of electron beam damage on the detection of indium-rich localisation centres in InGaN quantum wells using transmission electron microscopy

T. M. SMEETON, C. J. HUMPHREYS*, J. S. BARNARD, M. J. KAPPERS
Department of Materials Science and Metallurgy, University of Cambridge, Pembroke Street, Cambridge, CB2 3QZ, U. K.
E-mail: colin.humphreys@msm.cam.ac.uk

Published online: 17 April 2006

High-resolution transmission electron microscope (HRTEM) lattice fringe images and lattice parameter maps are used to reveal the rapid modification of InGaN quantum wells by the electron beam in a TEM. Images acquired within seconds of first irradiating a region of quantum well do not exhibit the strong nanometre-scale strain contrast which has been reported to signify the presence of very indium-rich regions in InGaN quantum wells. However, after a very short period of irradiation by a relatively low electron beam current density, images of the specimen could be interpreted as indicating the presence of these indium "clusters". The beam damage is shown to occur for the InGaN quantum wells grown in our lab as well as those in a commercial blue light emitting diode (LED) and in TEM specimens prepared only using mechanical polishing. Possible mechanisms for the beam damage are discussed and we make suggestions as to what may cause exciton localisation in quantum wells that do not contain gross composition fluctuations.

1. Introduction

Quantum wells of the $In_xGa_{1-x}N$ alloy are widely used as the active layers of optoelectronic devices such as blue and green light emitting diodes and blue-violet laser diodes [1]. A remarkable characteristic of these devices is that they can deliver very efficient light emission even when large densities of threading dislocations propagate into their active regions [2]. As in other compound semiconductors, threading dislocations in III-nitrides are known to act as non-radiative recombination centres [3–5]. However, InGaN-based devices can tolerate dislocation densities as much as several orders of magnitude higher than similarly efficient devices based on other semiconductor materials [2].

There has been huge interest in explaining the unusually small impact of dislocations on the optical properties of InGaN layers. Although the precise mechanism of luminescence is still a subject of active debate, there are strong indications that the light emission from InGaN quantum wells is dominated by the recombination of localised excitons e.g. [6]: soon after being formed, excitons become localised at low energy sites rather than remaining free to diffuse throughout the quantum well. Excitons localised in this way are much less likely to encounter a dislocation and recombine non-radiatively so the model does provide an explanation for the dislocation tolerance of the InGaN layers. Identifying the source of the localisation effects is considered crucial to fully understanding and exploiting the luminescence from the quantum wells. One possibility is that localisation occurs at local minima in the InGaN band gap which would be introduced by the presence of indium-rich regions. It is important, therefore, to determine whether InGaN quantum wells contain fluctuations in composition.

There is a tendency for phase separation within bulk InGaN layers. An early report suggested that although

*Author to whom all correspondence should be addressed.
0022-2461
DOI: 10.1007/s10853-006-7876-x

homogeneous InGaN epilayers could be formed over the full composition range, some of this material was metastable and prone to separate into indium-rich and indium-poor phases during prolonged annealing treatments [7]. More recently, thermodynamic studies have concluded that there is a miscibility gap in the $In_xGa_{1-x}N$ system and that for typical InGaN growth temperatures ($\sim$600–800°C) and typical quantum well compositions ($0.10 \leq x \leq 0.25$) the homogeneous alloy is either metastable or unstable, leading to decomposition e.g. [8]. Other thermodynamic studies have suggested that the phase separation may be suppressed somewhat for biaxially strained InGaN layers grown epitaxially on the (0001) surface of elastically relaxed GaN [9]. It remains unclear how closely these thermodynamic predictions apply to the non-equilibrium growth conditions used for most InGaN layers, however, experimental results on some thick ($\sim$200 nm) InGaN epilayer samples were shown to be consistent with phase separation occurring in InGaN films with indium fractions of 0.1 and above [10].

It was suggested that for quantum well growth the surface solubility of indium in InGaN may be more relevant than the lower bulk solubility and this might discourage phase separation [11]. There are, however, many reports of large composition fluctuations, and possibly phase separation, occurring in InGaN quantum wells. The reports of this indium "clustering" have been based mainly on the results of transmission electron microscopy (TEM) analysis of the layers. In the first reports of this effect, bright field TEM images of InGaN/GaN multiple quantum well (MQW) samples were shown to contain dark dot-like features with a size of $\sim$3 nm [12, 13]. Since the indium atom is much larger than the gallium atom, large fluctuations in InGaN composition will cause variations in the lattice strain and consequently variations in strain contrast in a TEM image. The dot-like features were therefore attributed to strain contrast caused by nanometre-scale fluctuations in the InGaN composition. This conclusion was reported to be further supported by energy dispersive X-ray spectroscopic analysis which indicated a correlation between the dark dots and higher indium contents [13]. Exciton localisation was attributed to the nanometre-scale indium-rich regions. It was pointed out in one of these papers [12] that the blotchy contrast could have been an artefact of the ion milling procedures used in TEM specimen preparation, where indium droplets can form on the sample surface under some conditions [14]. It has since been reported that contrast similar to that described in these early papers can definitely be seen as an artefact of specimen preparation [10, 15].

More recently, many high-resolution TEM (HRTEM) images of InGaN quantum wells have been published which show similar—but not identical—dot-like contrast which is not believed to be a consequence of any ion milling artefacts [e.g. 16–19]. As with the earlier images, these features have been attributed to strain contrast caused by nanometre-scale fluctuations in composition. The inhomogeneous strain has been investigated in a more quantitative manner using image analysis algorithms to extract local lattice parameter maps (LPMs) from HRTEM images [e.g. 20–24]. These lattice parameter maps showed small (typically $\sim$1–3 nm) regions with a much larger lattice parameter than the surrounding InGaN. For a range of samples grown by metalorganic vapour phase epitaxy (MOVPE) with mean compositions between $In_{0.09}Ga_{0.91}N$ and $In_{0.18}Ga_{0.82}N$, these lattice parameter maps were interpreted as indicating $\sim$3 nm inclusions with a composition of at least $In_{0.8}Ga_{0.2}N$, and perhaps approaching pure InN [21]. Pure InN inclusions with 1–3 nm size were reported to be consistent with similar HRTEM analysis of quantum wells grown by both MOVPE and molecular beam epitaxy (MBE) with mean compositions of about $In_{0.16}Ga_{0.84}N$ [25]. The presence of these very indium-rich regions has been widely used to explain the strong localisation of excitons in InGaN quantum wells.

In this paper we show that InGaN quantum wells are liable to rapid modification under the TEM electron beam and suggest that unless the beam damage artefacts are taken into account there is the potential to falsely infer the presence of nanometre-scale indium-rich regions from HRTEM data. HRTEM images and LPMs acquired using conditions chosen to identify and minimise the artefacts indicate composition fluctuations which are at most much weaker than those often reported by others. We point out that even without gross fluctuations in composition, the exciton localisation in the layers can still be rationalised either by the presence of weak composition fluctuations—which may be too small to be detected by HRTEM—or of small quantum well width fluctuations.

We have briefly described this electron beam damage before [26] and have since encountered suggestions that our results may apply only to InGaN grown on the MOVPE equipment in our laboratory or may be related to our TEM specimen preparation procedures, rather than being a general effect. Therefore, in addition to describing our earlier experiments in more detail, we also report further measurements which include studies of the electron beam sensitivity of InGaN quantum wells in a commercial blue LED and of TEM specimens prepared only using mechanical polishing.

2. Experimental details

InGaN/GaN quantum well samples were grown by MOVPE on *c*-plane sapphire in a $6 \times 2''$ Thomas Swan Close Coupled Showerhead reactor using trimethylgallium (TMG) and trimethylindium (TMI) as group-III metal sources and ammonia (NH_3) as the source of nitrogen. GaN layers were grown using a hydrogen carrier

gas and InGaN layers using a nitrogen carrier gas. A GaN nucleation layer with a nominal thickness of 30 nm and then a GaN epilayer with nominal thickness of 2 μm were grown at temperatures of 530 and 1030°C respectively. The threading dislocation density at the top of this film was about 1×10^9 cm^{-2}. A multiple quantum well sample with ten superlattice repeats consisting of a 2.8 nm thick $In_{0.22}Ga_{0.78}N$ quantum well and a 7.2 nm thick GaN barrier was then grown at 730°C. The layer thicknesses and compositions were measured using high-resolution X-ray diffraction as we have reported previously [27]. Detailed low-temperature photoluminescence studies of single quantum wells grown in the same way showed that the luminescence from these quantum wells was dominated by the recombination of excitons and also showed that the localisation occurred on a length scale of about 1–3 nm [28].

Wedge-shaped cross-sectional TEM specimens were prepared by tripod polishing on diamond lapping mats. A wedge angle of $\sim 3^\circ$ was used for the MQW sample and the InGaN/GaN material at the thin end was reduced to electron transparency. Specimens for HRTEM analysis were thinned further by ion milling (Gatan PIPS; 3.2 keV argon ions). The ion guns were incident on the sample at angles of $\pm 4^\circ$ relative to the wedge surfaces and the total milling time was less than ten minutes. For the commercial blue LED sample, a wedge angle of $\sim 7^\circ$ was used, the specimen was mechanically thinned to a thickness of a few microns and then ion milled for several hours using the conditions described above. Heating of the specimen was minimised by use of a relatively low-energy ion beam and limiting the gun activity to three out of every ten seconds. No indium droplets [12, 14, 15] were observed on the specimen surfaces during subsequent TEM analysis. Energy-filtered TEM was used to estimate the thickness of the specimens and all HRTEM images were acquired from specimens less than 20 nm thick.

HRTEM images were obtained using an FEI Tecnai F20 G2 with a 200 keV Schottky field emission gun electron source and a point-to-point resolution of 0.25 nm. (0002) lattice fringe images were acquired with the incident electron beam tilted so that the undiffracted and (0002) diffracted beams were each an equal angle away from the optic axis of the microscope. The specimen was oriented so that the incident beam travelled perpendicular to the [0001] direction and at an angle of 6°–7° to a $\langle 11\bar{2}0 \rangle$ axis. Under these conditions the (0002) and$(000\bar{2})$ reflections were under equal excitation and only the undiffracted and (0002) beams were used to form the image. Images were recorded using a 1 k $\times$ 1 k charge coupled device. The bright field images in Fig. 4 were acquired using a Philips CM30 TEM with a 300 keV LaB_6 thermionic electron source.

For measurements showing the time-dependence of the HRTEM image contrast, the camera was programmed to acquire a series of images with a fixed delay between each exposure. Specimen drift between images in each series was subsequently corrected off-line. The incident electron beam current density chosen for the experiments was substantially below the highest attainable from the microscope and close to the minimum compatible with HRTEM imaging, in that it just allowed an image to be acquired in an exposure time during which mechanical drift of the specimen was inconsequential. Based on a measurement of the total current in the beam, the current density incident on the sample was estimated to be (35 $\pm$ 20) A cm^{-2} for all of the data.

A freshly prepared TEM specimen was used for each experiment and great care taken to avoid any irradiation of the quantum well material during alignment of the microscope. In spite of these precautions, a small amount of irradiation of the material of interest was almost inevitable during navigation of the specimen. The first images shown in each series were acquired as soon as possible after first intentionally exposing a region of InGaN quantum well to the electron beam. To achieve this, all imaging parameters were first optimised using neighbouring GaN that was at a similar orientation and height. InGaN layers were then brought under the electron beam, the mechanical drift was allowed to stabilise and any necessary adjustments to the imaging conditions were made before the first image was acquired.

Local lattice parameter maps (LPMs) were extracted from lattice fringe images using a process similar to the DALI technique [21]. Our implementation of this procedure used image analysis algorithms to determine the positions of the (0002) lattice fringes in the image and then calculate a two-dimensional map of the lattice fringe separation. We did not use Fourier filtering of the image prior to this process. HRTEM image simulations [29] were used to confirm that for our imaging conditions there was a direct correspondence between the lattice fringe spacing in the image and the lattice plane spacing in the specimen so that fringe spacing maps can be treated as LPMs.

3. Results

A (0002) lattice fringe image of three of the $In_{0.22}Ga_{0.78}N$/GaN quantum wells in the MQW sample is shown at the top left of Fig. 1. The image was acquired 20 s after this region of the specimen was intentionally brought under the electron beam for the first time. The image intensity in the InGaN layers is largely uniform but there are a few definite contrast variations and two of these have been arrowed. The remainder of Fig. 1 shows the evolution of the HRTEM image contrast over the subsequent 540 s exposure to the low electron beam current density. It is clear that the specimen was substantially modified by the electron beam irradiation. During the first couple

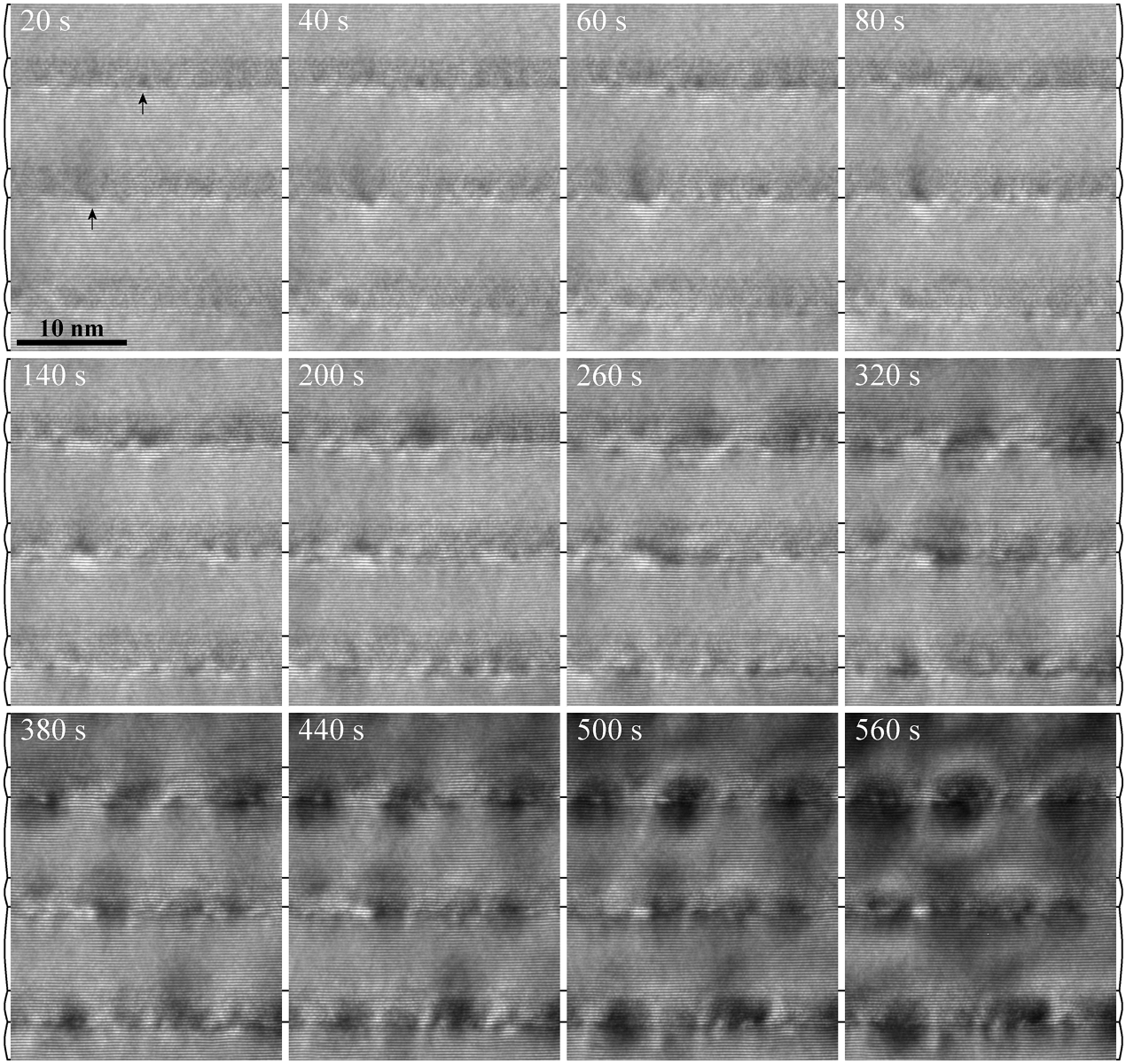

Figure 1 A series of (0002) HRTEM lattice fringe images of three quantum wells in the $In_{0.22}Ga_{0.78}N$/GaN MQW sample. The images were acquired after exposure of the specimen to an electron beam flux of ~ 35 A cm^{-2} for the labelled times. The positions of the quantum well interfaces are indicated by the horizontal lines; the growth direction was from the bottom to the top of the page.

of minutes some strong contrast fluctuations developed in the InGaN layers and after several minutes the images were dominated by lobes of contrast centred around the bottom interface of each quantum well. Similar contrast evolution was observed during exposure of other regions of the same quantum well sample to incident beam energies of 300 keV and 400 keV [26].

The effect of electron beam irradiation on the LPMs extracted from (0002) lattice fringe images of one InGaN quantum well in the same sample is shown in Fig. 2. The contoured grey-scale images show the value of δ which is defined as the local (0002) lattice spacing divided by the mean GaN (0002) lattice spacing in the barrier layers on either side. The estimates of indium fraction, x, included in the figure give an indication of the $In_xGa_{1-x}N$ composition that would be expected to have the corresponding lattice spacings. These were calculated assuming the InGaN layer was biaxially strained to GaN in the (0001) plane and using a Vegard's law interpolation for the alloy lattice parameters and elastic constants [27]. To allow as much of the quantum well length as possible to be included in the figure, the mechanical drift between images in the series was not corrected in the vertical direction and is indicated by the dashed line. The final few frames in the series show that significant artefacts were introduced to the LPMs after 180 s of exposure to the low current density electron

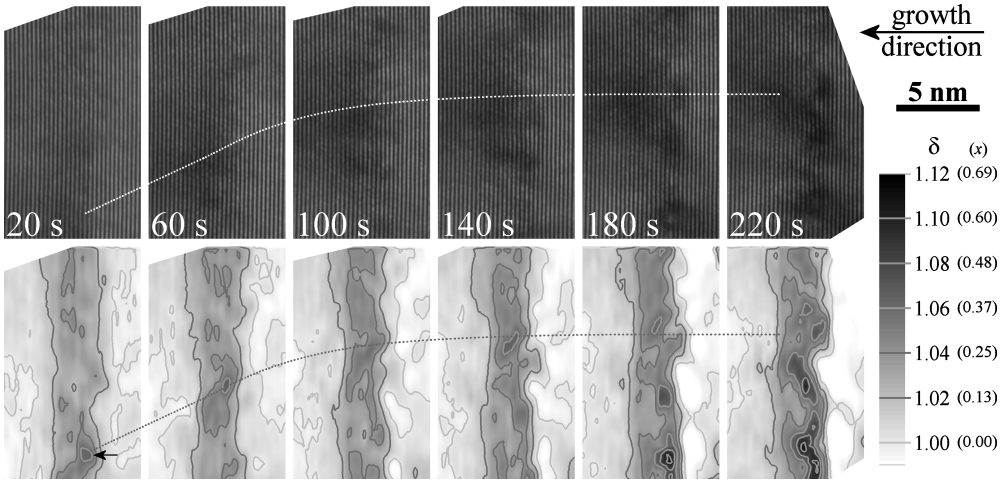

Figure 2 A series of (0002) HRTEM lattice fringe images (top row) and lattice parameter maps derived from them (bottom row) of one quantum well in the $In_{0.22}Ga_{0.78}N$/GaN MQW sample. The images were acquired after exposure of the specimen to an electron beam flux of ~ 35 A cm^{-2} for the labelled times. A vertical drift between adjacent images is indicated by the dotted line which passes through the same position in the sample mid-way across each frame.

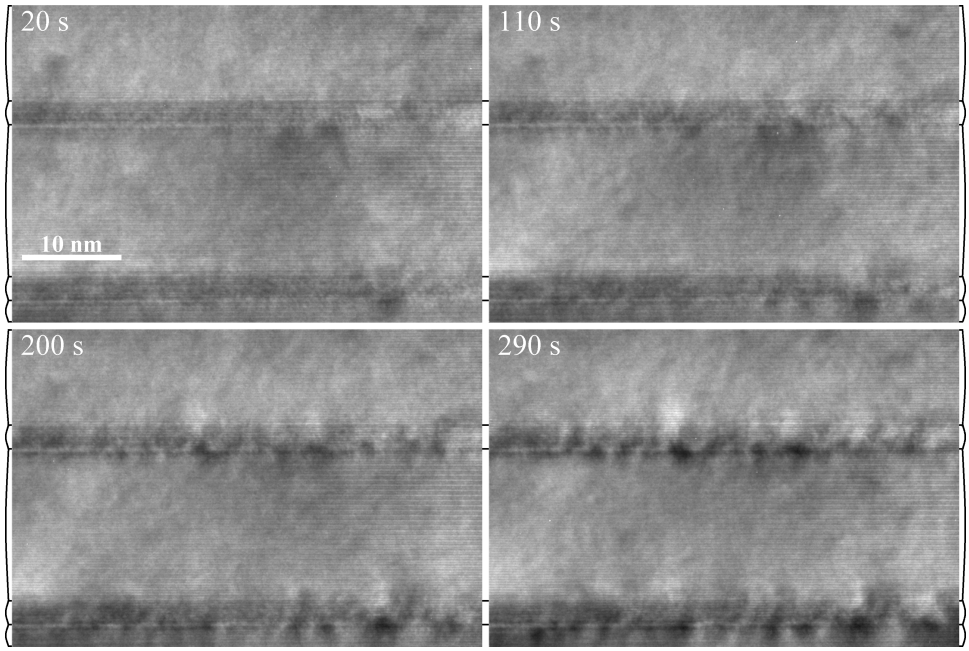

Figure 3 A series of (0002) HRTEM lattice fringe images of two quantum wells in the commercial blue (electroluminescence peak wavelength of 470 nm) LED. The images were acquired after exposure of the specimen to an electron beam flux of ~ 35 A cm^{-2} for the labelled times. The positions of the quantum well interfaces are indicated by the horizontal lines; the growth direction was from the bottom to the top of the page.

beam. These artefacts took the form of local regions with a much higher lattice parameter than the neighbouring InGaN. The correlation between lattice plane spacing and estimated indium fraction may be invalid for these later images and this is discussed in more detail below.

HRTEM images of the InGaN quantum wells in the commercial blue LED are shown in Fig. 3. The top left image was acquired after this region of the specimen had been intentionally exposed to the electron beam for 20 s and the remaining three images show the evolution over the next 270 s. The electron beam current density was similar to that used to obtain the data in Fig. 1 and a number of direct comparisons can be drawn between the evolution of contrast in the two cases. Again, the lowest-dose image exhibits some small contrast inhomogeneities, the subsequent images show much more substantial contrast variations and these were centred around the bottom interface of each quantum well.

Although relatively low ion-beam energies were used during the ion milling of the TEM specimens imaged in

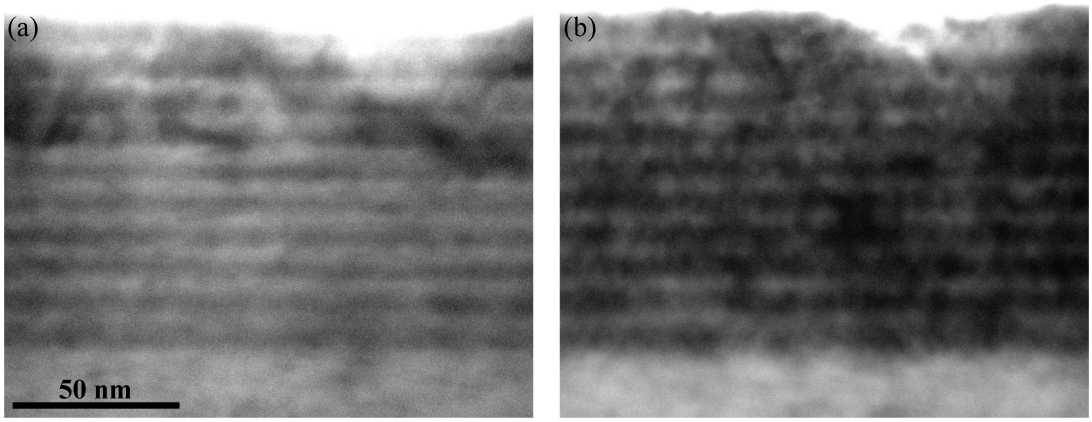

Figure 4 Bright field TEM images of the quantum wells in the $In_{0.22}Ga_{0.78}N$/GaN MQW sample in a TEM specimen thinned using only mechanical polishing. (a) acquired following minimal electron beam irradiation; (b) the same location after several minutes of irradiation by the electron beam.

the three figures above, it was important to determine whether the milling conditions were causing the sensitivity of the InGaN quantum wells to rapid damage. Hence, a specimen was prepared using *only* mechanical thinning and TEM images of this MQW sample are shown in Fig. 4. The bright field image in Fig. 4a was acquired after minimal electron beam dose and, although the image quality was poor because the specimen was relatively thick and suffered from substantial surface damage associated with the mechanical polishing, the individual quantum well layers could be distinguished. The image in Fig. 4b shows the same part of the quantum wells after several minutes of exposure to the electron beam. The modification of the quantum well contrast from relatively uniform intensity to dot-like variations is similar to the behaviour illustrated in Fig. 1. This suggests that the susceptibility to electron beam damage is intrinsic to the InGaN/GaN quantum well structures and not a consequence of our ion milling procedures.

4. Discussion

4.1. HRTEM measurement of indium composition fluctuations

The behaviour illustrated in the four figures above shows the strong tendency for InGaN quantum wells to be modified during irradiation by the electron beam in a TEM. In Figs 1–3, the electron beam damage was shown to cause contrast variations which are indicative of a nanometre-scale strain inhomogeneity within the InGaN layers. The LPMs in Fig. 2 provide a more quantitative measure of this effect with the final two frames showing $\sim$2 nm sized strain features having a much greater lattice parameter than the neighbouring InGaN.

Nanometre-scale fluctuations in the indium fraction of the quantum wells are expected to cause effects very similar to what is shown in these results to be caused by the incident electron beam. It is obvious that if any of our HRTEM images or LPMs acquired after a couple of minutes exposure to the electron beam were used in isolation, and without consideration of the beam damage effects, then they would give a false indication of the strain distribution—and therefore the composition distribution—in the as-grown quantum well. We stress that the measurements presented above were obtained using a relatively low electron beam current density. We suggest, therefore, that it is essential that electron-beam induced artefacts are taken into account in any attempt to detect indium composition fluctuations in InGaN quantum wells.

The lowest dose images in Figs 1 and 3 both exhibit intensity fluctuations which suggest that significant lattice distortions were already present at a very early stage. The key question is whether these fluctuations were present in the as-grown material or are attributable to the early stages of beam damage. The two strongest fluctuations in intensity in the first image in Fig. 1 are arrowed and inspection of the subsequent few images in the series shows that strain contrast due to beam damage effects rapidly developed at precisely these two sites. Close inspection reveals that all of the other intensity fluctuations in the lowest dose images of Figs 1 and 3 can be linked with subsequent beam damage features. The continuous evolution of all of the intensity fluctuations proves that the InGaN quantum wells were undergoing substantial modification *immediately* after the first image. This means that we cannot rule out that modification was also occurring before the first image and that the lattice distortions responsible for the intensity fluctuations in this image simply result from the initial stages of beam damage. We conclude, therefore, that the lowest-dose images in Figs 1 and 3 can only be used with confidence as an indication of the upper limit of any strain inhomogeneities present in the as-grown material, and not as a faithful indicator of the original quantum well nanostructure.

LPMs are sensitive to smaller lattice distortions which are not immediately apparent in the unprocessed HRTEM images. The lowest dose data in Fig. 2 reveals one strain

feature (arrowed) where the lattice parameter was locally higher than in the neighbouring InGaN material. This fluctuation, although much weaker than those present in the later images in the series, was still significant above the noise in the measurement (the noise is determined from the apparent lattice parameter fluctuations in the adjacent GaN layers). The size and strength of the feature is not substantially modified in the subsequent few images of the series and this might indicate that it was independent of the beam damage occurring elsewhere in the quantum well. In low-dose LPM studies of several InGaN quantum well samples we have seen some similar features and, in some cases, the fluctuation of δ from its mean in the InGaN layers was as much as 20% higher than the noise (typically an average deviation of δ from its mean by about 0.003). These fluctuations in δ are substantially smaller than have been reported in the literature for InGaN quantum wells by others (compare with the maximum values of δ of 1.10 in $In_{0.18}Ga_{0.82}N$ [21] and $In_{0.2}Ga_{0.8}N$ [24] quantum wells), but if we could be certain that they were independent of beam damage then they might indicate the presence of nanometre-scale fluctuations in the indium composition of the quantum wells. Since our other results indicate that the InGaN quantum wells undergo modification within the earliest stages of irradiation, however, we must conclude that these fluctuations in strain could also be due to the electron beam damage.

4.2. Mechanism of the electron-beam-induced strain

Two mechanisms by which the electron beam may have modified the InGaN quantum well specimens are radiolysis and knock-on damage. In radiolysis, the primary damage process is ionisation by the incident electron beam: the energy released during the relaxation of ionised atoms is converted into kinetic energy of displaced atoms [30]. Knock-on damage involves the direct transfer of energy and momentum from the incident electrons to displace atoms. Knock-on displacement of gallium or indium atoms in the InGaN lattice is unlikely for a 200 keV electron beam but the relatively light nitrogen atoms are more susceptible [31, 32]. Knock-on of nitrogen both in GaN [33] and InN [34] has been reported for 100 keV incident electrons. In light of these results, displacement of nitrogen in InGaN layers seems highly probable at the higher beam energy of 200 keV used in this work.

There are two possible explanations for the strain inhomogeneities apparent in the HRTEM images. The first is that they could have been caused by the generation of increasing numbers of vacancies or interstitials either through radiolysis or knock-on. Aggregation of these point defects can be energetically favourable [31] and the resulting lattice distortion can cause strong local strain contrast [35] which is similar to that present in the images of the beam damaged quantum wells. Furthermore, if the point defects carried a net charge and migrated under the action of the intrinsic electric field in the quantum well, this might explain the apparent concentration of the electron-beam-induced strain at the bottom (the $(000\bar{1})$ nitrogen-face) of the InGaN layers. If atomic displacement were the origin of the modification of the specimen then the correlation between lattice spacing and InGaN composition listed in Fig. 2 would not apply in beam damaged quantum wells.

The second possible cause of the strain contrast is the electron-beam-induced redistribution of indium within the quantum well layers. This would be expected due to the thermodynamic instability of the InGaN alloy: for temperatures below about 700°C, thermodynamic calculations indicate that the $In_{0.22}Ga_{0.78}N$ layers in the MQW sample would be liable to spinodal decomposition into very indium-rich and very indium-poor phases [8]. If the interaction of the electron beam with the specimen increased the diffusion rate to allow the kinetic barrier to this reaction to be overcome, then phase separation would occur. The temperature of a TEM specimen rises during irradiation by the electron beam and this will increase the diffusion rates. The temperature rise depends on the efficiency with which thermal energy is dissipated from the irradiated region. Based on reported values of the thermal conductivities of the GaN epilayer and sapphire substrate in the MQW sample of 100 $Wm^{-1}\,K^{-1}$ and 30 $Wm^{-1}\,K^{-1}$ respectively [36], the rise in temperature of the specimen under the electron beam should be no more than a few kelvin [31, 32]. It is unlikely that such moderate heating could have affected the diffusion rate sufficiently to cause the rapid modification of the specimen. It is possible, however, that a radiolysis mechanism might exist through which the weakening of bonds caused by electron-beam-induced ionisation events increased the rate of diffusion. Alternatively, any displacement of atoms from their lattice sites by the electron beam could have increased the rate of diffusion of the indium and gallium atoms in the lattice.

Unfortunately, our results do not allow us to distinguish between the two possibilities of beam-induced vacancy formation and beam-induced redistribution of indium. It is known that irradiation of 6H-SiC with 100–300 keV TEM electron beams causes point defect generation due to displacement of carbon atoms [37] and similar behaviour may be expected in III-nitrides. Additionally, it has been reported that during TEM-based cathodoluminescence studies of InGaN quantum wells there was a decrease in the luminescent intensity during irradiation by 120 keV electrons [38]. This suggests the electron irradiation introduces non-radiative recombination centres and indicates that the generation of point defects is significant in the InGaN beam damage mechanism.

4.3. Indium composition fluctuations and localisation

We have shown that the fluctuations of composition in the InGaN quantum wells we have analysed are at most substantially smaller than has frequently been reported for similar material. Indeed, it is possible that all indicators of composition fluctuations in our lowest electron-dose images are due to beam damage and that the as-grown quantum wells are homogeneous. Since the quantum wells show evidence of strong exciton localisation, we end by considering what would cause localisation in the absence of the gross composition fluctuations to which it is usually attributed.

A crucial point is that due to the very large rate of change of the InGaN band gap with indium fraction, strong exciton localisation could be caused by composition fluctuations which are probably far too weak to be detected by HRTEM. For $0 < x < 0.23$, the variation in $In_xGa_{1-x}N$ band gap with composition is given by $dE_g/dx = -3.91$ eV [39]. An increase in indium fraction by just one atomic percent causes the bulk band gap to decrease by an amount greater than the thermal energy at room temperature ($kT \approx 26$ meV). Thus fluctuations in InGaN quantum well composition of just a few atomic percent may be capable of causing room temperature localisation effects. Photoluminescence studies have suggested that excitons were localised in our InGaN quantum wells on a length scale of a few nanometres [28]. Even without the complication of beam damage artefacts, it would be very difficult to detect such small fluctuations in composition at this nanometre-scale using TEM because of the averaging effects of projection through the specimen thickness.

Even completely random alloy disorder is a plausible cause of localisation. The fluctuations in conduction and valence band energies caused by alloy disorder scale with dE_g/dx [40]. The very large value for this rate of change in InGaN (compared with most other semiconductor alloys) could be sufficient to account for room temperature localisation effects [41]. Simple calculations show that if indium atoms are distributed randomly in an $In_{0.2}Ga_{0.8}N$ alloy lattice then the local composition, averaged over an exciton radius and localisation length-scale of about 3 nm, fluctuates by several atomic percent.

Local increases in the thickness of InGaN quantum wells are an alternative source of localisation since they effectively cause the separation between electron and hole energy levels to be reduced due to weaker quantum confinement effects and the quantum confined Stark effect [6]. It has been suggested that a change in InGaN quantum well width by a single monolayer (~ 0.25 nm) could cause strong localisation effects [42]. Z-contrast high-resolution scanning TEM results for our quantum wells suggested that the top InGaN-GaN interface can exhibit a roughness with an amplitude of about one monolayer [28]. This roughness causes monolayer well-width fluctuations so may account for the exciton localisation effects.

5. Conclusions

We have shown that InGaN quantum wells are extremely sensitive to damage by the electron beam in a TEM. We suggest that unless beam damage effects are taken into account when using HRTEM to study InGaN quantum wells, there is the potential to falsely infer the presence of strong indium composition fluctuations. The extreme electron beam sensitivity described here seems to be a general effect: it was found to occur for both InGaN quantum wells grown using conventional growth conditions in our commercial MOVPE reactor *and* in commercial blue LED quantum wells grown elsewhere; it was observed for all commonly used TEM beam energies (200–400 keV); and shown to happen independently of TEM specimen preparation (ion milling) procedures. The results suggest that images acquired after only 20 s exposure to an abnormally low electron beam current density may already exhibit beam damage, and that after at most a few minutes of exposure to this weak electron beam the images were, without question, significantly influenced by the electron irradiation. Very low dose electron imaging seems essential for reliable studies of any as-grown composition fluctuations in InGaN quantum wells.

Any composition fluctuations indicated by the low-dose HRTEM images and LPMs are, at most, significantly smaller than those often reported for InGaN quantum wells in the literature. Due to the rapid modification of the material by the electron beam, even our data acquired after a minimal electron dose can only be used to infer an upper limit for the extent of composition fluctuations in the as-grown quantum wells. It remains possible that all indications of strain inhomogeneities in these lowest-dose images are artefacts of the beam damage effect. If this is the case, exciton localisation can still be explained by the presence either of nanometre-scale fluctuations in composition of a few atomic percent, perhaps due to the random alloy disorder in a homogeneous quantum well, or fluctuations in well width of the order of a single monolayer.

Acknowledgments

We are grateful to the Engineering and Physical Sciences Research Council, Sharp Laboratories of Europe Ltd., Thomas Swan Scientific Equipment Ltd., The Isaac Newton Trust and FEI Company for funding.

References

1. S. NAKAMURA and S. CHICHIBU (Eds) "Introduction to Nitride Semiconductor Blue Laser and Light Emitting Diodes" (Taylor & Francis, London, 2000)

2. S. NAKAMURA, *Science* **281** (1998) 956.
3. *Idem*., *Semiconduct. Sci. Technol.* **14** (1999) R27.
4. S. J. HENLEY and D. CHERNS, *J. Appl. Phys.* **93** (2003) 3934
5. P. GIBART, *Reports of Progress in Phys.* **67** (2004) 667.
6. S. CHICHIBU, T. SOTA, K. WADA and S. NAKAMURA, *J. Vac. Sci. Technol. B* **16** (1998) 2204.
7. K. OSAMURA, S. NAKA and Y. MURAKAMI, *J. Appl. Phys.* **46** (1975) 3432.
8. I. HO and G. B. STRINGFELLOW, *Appl. Phys. Lett.* **69** (1996) 2701
9. L. K. TELES, J. FURTHMÜLLER, L. M. R. SCOLFARO, J. R. LEITE and F. BECHSTEDT, *Phys. Rev. B* **62** (2000) 2475.
10. F. A. PONCE, S. SRINIVASEN, A. BELL, L. GENG, R. LIU, M. STEVENS, J. CAI, H. OMIYA, H. MARUI and S. TANAKA, *Phys. Stat. Sol. (b)* **240** (2003) 273.
11. L. BELLAICHE, T. MATTILA, L.-W. WANG, S.-H. WEI and A. ZUNGER, *Appl. Phys. Lett.* **74** (1999) 1842
12. S. CHICHIBU, T. AZUHATA, T. SOTA and S. NAKAMURA, *ibid.* **69** (1996) 4188.
13. Y. NARUKAWA, Y. KAWAKAMI, M. FUNATO, S. FUJITA, S. FUJITA and S. NAKAMURA, *ibid.* **70** (1997) 981.
14. N. G. CHEW and A. G. CULLIS, *Ultramicroscopy* **23** (1987) 175.
15. A. N. WESTMEYER and S. MAHAJAN, *Appl. Phys. Lett.* **79** (2001) 2710.
16. Y.-S. LIN, K.-J. MA, C. HSU, S.-W. FENG, Y.-C. CHENG, C.-C. LIAO, C. C. YANG, C.-C. CHOU, C.-M. LEE and J.-I. CHYI, *ibid.* **77** (2000) 2988.
17. H. K. CHO, J. Y. LEE, N. SHARMA, C. J. HUMPHREYS, G. M. YANG, C. S. KIM, J. H. SONG and P. W. YU, *ibid.*. **79** (2001) 2594.
18. M. G. CHEONG, S. M. JEONG, H. S. YOON, C. S. KIM, R. J. CHOI, E. J. HWANG, E.-K. SUH and H. J. LEE, *J. Korean Phys. Soc.* **40** (2002) 300.
19. K. JACOBS, B. VAN DAELE, M. R. LEYS, I. MOERMAN and G. VAN TENDELOO, *J. Cryst. Growth* **248** (2003) 498.
20. C. KISIELOWSKI, Z. LILIENTAL-WEBER and S. NAKAMURA, *Japanese J. Appl. Phys.* **36** (1997) 6932.
21. D. GERTHSEN, E. HAHN, B. NEUBAUER, A. ROSENAUER, O. SCHÖN, M. HEUKEN and A. RIZZI, *Phys. Stat. Sol. (a)* **177** (2000) 145.
22. D. GERTHSEN, B. NEUBAUER, A. ROSENAUER, T. STEPHAN, H. KALT, O. SCHÖN and M. HEUKEN, *Appl. Phys. Lett.* **79** (2001) 2552.
23. D. GERTHSEN, E. HAHN, B. NEUBAUER, V. POTIN, A. ROSENAUER and M. SCHOWALTER, *Phys. Stat. Sol. (c)* **0** (2003) 1668.
24. Y.-C. CHENG, E.-C. LIN, C.-M. WU, C. C. YANG, J.-R. YANG, A. ROSENAUER, K.-J. MA, S.-C. SHI, L. C. CHEN, C.-C. PEN and J.-I. CHYI, *Appl. Phys. Lett.* **84** (2004) 2506.
25. P. RUTERANA, S. KRET, A. VIVET, G. MACIEJEWSKI and P. DLUZEWSKI, *J. Appl. Phys.* **91** (2002) 8979.
26. T. M. SMEETON, M. J. KAPPERS, J. S. BARNARD, M. E. VICKERS and C. J. HUMPHREYS, *Appl. Phys. Lett.* **83** (2003) 5419.
27. M. E. VICKERS, M. J. KAPPERS, T. M. SMEETON, E. J. THRUSH, J. S. BARNARD and C. J. HUMPHREYS, *J. Appl. Phys.* **94** (2003) 1565.
28. D. M. GRAHAM, A. SOLTANI-VALA, P. DAWSON, M. J. GODFREY, T. M. SMEETON, J. S. BARNARD, M. J. KAPPERS, C. J. HUMPHREYS and E. J. THRUSH, *ibid.* **97** (2005) 103508.
29. E. J. KIRKLAND, "Advanced Computing in Electron Microscopy" (Plenum Press, New York, 1998).
30. R. F. EGERTON, P. LI and M. MALAC, *Micron* **35** (2004) 399.
31. L. W. HOBBS, "Radiation effects in analysis of inorganic specimens by TEM" in "Introduction to Analytical Electron Microscopy," edited by J. J. HREN, J. I. GOLDSTEIN and D. C. JOY (Plenum Press, New York, 1979).
32. D. B. WILLIAMS and C. B. CARTER, "Transmission electron microscopy: a textbook for materials science" (Plenum, London, 1996).
33. T. J. EUSTIS and J. SILCOX, *Microscopy and Microanalysis* (1999) 642.
34. K. A. MKHOYAN and J. SILCOX, *Appl. Phys. Lett.* **82** (2003) 859.
35. M. L. JENKINS and M. A. KIRK, "Characterization of radiation damage by transmission electron microscopy" (Institute of Physics Publishing, Bristol, 2001)
36. J. ZOU, D. KOTCHETKOV, A. A. BALANDIN, D. I. FLORESCU and F. H. POLLAK, *J. Appl. Phys.* **92** (2002) 2534.
37. G. A. EVANS, J. W. STEEDS, L. LEY, M. HUNDHAUSEN, N. SCHULZE and G. PENSL, *Phys. Rev. B* **66** (2002) 035204.
38. N. M. BOYALL, K. DUROSE and I. M. WATSON, *Mater Res Soc Symposium Proceed* **743** (2003) L11.13
39. R. W. MARTIN, P. R. EDWARDS, K. P. O'DONNELL, E. G. MACKAY and I. M. WATSON, *Phys. Stat. Sol. (a)* **192** (2002) 117.
40. S. D. BARANOVSKIĬ and A. L. ÉFROS, *Sov. Phys. Semicond.* **12** (1978) 1328.
41. H. X. JIANG, J. Y. LIN and W. W. CHOW, "Time resolved photoluminescence studies of III-nitrides" in "III-nitride semiconductors: optical properties I," edited by M. O. MANASREH and H. X. JIANG, (Taylor and Francis, London, 2002)
42. A. SOLTANI-VALA, M. J. GODFREY and P. DAWSON, *Phys. Stat. Sol. (b)* **228** (2001) 453.